OPEN ACCESS
International Journal of Structural Stability and Dynamics
Vol. 26, No. 19 (2026) 2641003 (21 pages)

DOI: 10.1142/S0219455426410038

World Scientific
www.worldscientific.com

A Preliminary Evaluation of a Concept of Multiple Cold Water Pipe System for a Floating OTEC Plant

Ryoya Hisamatsu* and Tomoaki Utsunomiya†

Department of Marine Systems Engineering, Kyushu University
Motooka 744, Nishi-ku, Fukuoka 819-0395, Japan
**hisamatsu@nams.kyushu-u.ac.jp*
†*utsunomiya@nams.kyushu-u.ac.jp*

Received 30 April 2025
Accepted 17 March 2026
Published 9 April 2026

Ocean Thermal Energy Conversion (OTEC) has been attracting attention for its stability and potential for integration with deep seawater utilization. For a Floating OTEC plant, developing an ultra-large-diameter Cold Water Pipe (CWP) has long been a major challenge. This preliminary study explores the economics, structural performance, and design feasibility of a concept of multiple CWP system for floating OTEC. As a case study, a baseline design comprising a ship-shaped platform, a spread mooring system, and a GFRP CWP is considered. The economics of multiple CWPs are evaluated by varying the diameter, flow velocity, and number of pipes while maintaining a constant flow rate. The results revealed that, for each pipe configuration, there exists an optimal combination of diameter and flow velocity, and that the economic impact associated with adopting multiple CWPs is negligible when optimal designs are considered. Furthermore, the dynamic characteristics of the coupled platform–mooring–CWP system under extreme environmental conditions are investigated using the optimal design candidates. Time-domain simulations confirm that the concept using multiple CWPs is technically feasible for floating OTEC applications.

Keywords: OTEC; cold water pipe; floating structure; dynamic analysis.

1. Introduction

The Ocean Thermal Energy Conversion (OTEC) system produces electricity by driving a thermodynamic cycle driven by the temperature difference between the surface and deep layers of the ocean.[1] Owning to the high temporal stability of

*Corresponding author.

the temperature difference, OTEC can supply renewable and stable power to the electrical grid, similar to geothermal energy and hydroelectric power. In addition, OTEC has been recognized for its potential to deliver an additional benefits through integrating with other industries such as desalination, green hydrogen production, seawater air conditioning, ocean nutrient enhancement, and other applications utilizing deep seawater.[2,3]

At present, onshore plants are being deployed on tropical islands and in Small Island Developing States (SIDSs). On the other hand, it is widely recognized that the costs associated with deep seawater intake and discharge facilities for onshore plants will increase significantly with the scaling-up of plant capacity. In consequence, the development of floating plant technology will be essential for deploying over 10 MW outputs.[4] Furthermore, floating OTEC plants are predicted to have economies of scale; thus, the cost of energy can be reduced by increasing the output from a floating plant. A 100 MW-scale plant has been positioned as a target toward commercializing OTEC.[4] This study focuses on the engineering problems of 100 MW-scale floating plants.

Floating OTEC has been studied in many fields: conceptualization,[5–9] economics,[10] and global potential.[11] Focusing on structural engineering, floating structures, mooring systems, power cables, water pipelines, and their integration have been studied. Among them, the floating structure, mooring, and power cable share common technologies with other offshore industries, such as offshore oil and gas and offshore wind. On the other hand, the Cold Water Pipe (CWP), generally specified as a deep-seawater intake pipe, is a unique component in commercial-scale floating OTEC plants and remains a technical challenge. Utilizing a small temperature difference theoretically requires a large flow rate of the heat source; therefore, an OTEC plant requires deep seawater with a flow rate of 2–3 m^3/s per 1 MW output. To satisfy the flow rate requirement, the CWP has been historically designed to have a very large diameter.

OTEC technology was rapidly developed in the 1970s, triggered by the oil crisis in 1973. The progress of this period has been summarized in the literature.[12] The US Department of Energy (DOE) systematically evaluated 67 design candidates of the CWP for a 100–400 MW floating plant with regard to their manufacturability, economics, and risk.[13] As a result, a Fiber-Reinforced Plastic (FRP) walled pipe hanging from a floating platform was ranked the best candidate for the structural design of the CWP. Subsequently, this structural type was demonstrated in a small scale at-sea test by Nihous and Vega.[14] More recently, the Lockheed Martin group reported the development of a manufacturing method for the FRP pipe at a floating platform.[15] Meanwhile, several at-sea demonstration plants have adopted High-Density Polyethylene (HDPE)[16] or steel[17] for the CWP with a diameter of 1–2 m.

Simultaneously, the static and dynamic analysis of the CWP has been studied in a number of research and development projects. In the 1980s, Pauling[18] developed the FEM code for the frequency-domain analysis of the coupled behavior

between the floating structure and the CWP. The code was validated by comparing it with two other codes,[19] a wave tank test[20] and at-sea demonstration.[14] These studies highlighted the importance of the dynamic interaction between the CWP and the floating structure. Accordingly, tentative technical standards regarding OTEC include the requirement to evaluate the coupled behavior.[21,22] In recent years, the structural performance of the CWP can be evaluated using time-domain dynamic analysis tools standardized in the offshore industry. Besides, low-fidelity methods such as frequency-domain analysis are still a useful tool for comprehensively exploring the design space as in Hisamatsu and Utsunomiya.[23]

To verify the analysis codes, several model tests have been reported. The model tests can be categorized into wave tank tests using assembly models with floating structures[24,25] and single-unit tests of the CWP.[26–30] Recently, research on the latter model tests has focused on the fundamental understanding of the internal flow effects, Vortex Induced Vibration (VIV), and their integration.

Most aforementioned studies are based on the design of a single large-diameter CWP. However, several studies on the economics of OTEC have recently discussed concepts employing multiple CWPs within a currently available diameter range to avoid the high initial cost, technical difficulties and uncertainties in cost estimation.[31,32] Although this approach is inferior in terms of hydraulic head loss, it has been suggested that the economic impact is comparatively small. Therefore, understanding the technical feasibility and the structural performance of a concept of multiple-CWP system would be helpful in improving the accuracy of cost estimation.

The purpose of this study is to understand the design trade-offs and structural performance of a floating platform with multiple CWPs. In this paper, a baseline design of a 100 MW plantship is first defined as a study case. Then, the design trade-offs of the CWP are discussed by varying the number, diameter and flow velocity. Simultaneously, their dynamic response characteristics are evaluated using a low-fidelity coupled model. Subsequently, time-domain analysis is performed for several design candidates to discuss their design feasibility.

2. Baseline Design Definitions

This section presents the definition of a baseline design of an OTEC plantship. This concept was originally proposed by Nihous and Vega.[5] Subsequently, concepts reflecting knowledge of Floating Production Storage and Offloading (FPSO) systems from offshore oil development have been proposed by SBM[33] and Adiputra *et al.*[9] This research is based on the latter concept, as shown in Fig. 1. This design is expected to be superior in terms of economics since it can utilize a pre-owned ship. This concept would be suitable for sites where there is a sufficient temperature difference above 20°C and no tropical typhoons, e.g. Indonesia.

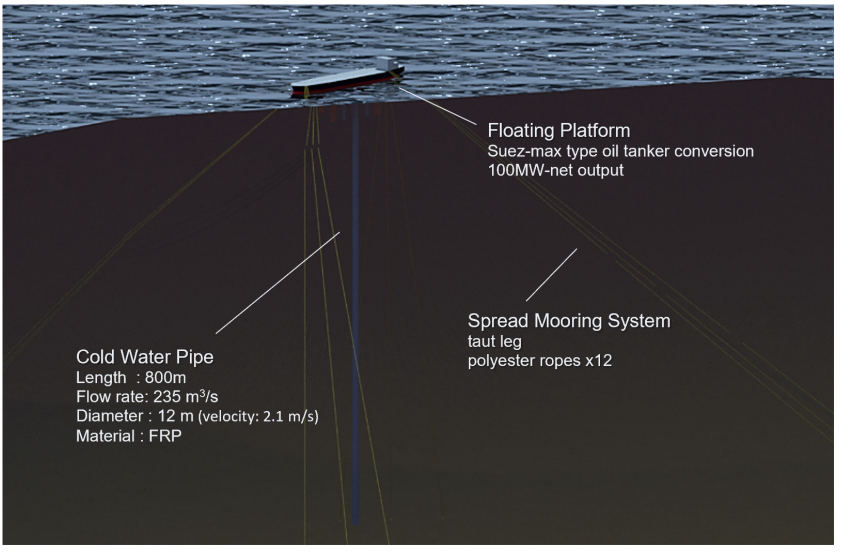

Fig. 1. Conceptual sketch of the OTEC plantship.

Table 1. Main properties of the 100 MW plantship.

Properties	Value
Power generation (gross)	143 MW
Power generation (net)	100 MW
Warm water temperature	29°C
Cold water temperature	7°C
Flow rate of warm water	470 m^3/s
Flow rate of cold water	235 m^3/s

As the design conditions for power generation, the surface seawater temperature is 29°C and the deep seawater temperature is 7°C at a depth of 800 m. Adiputra *et al.*[9] estimated the system configuration, flow-rate requirements, and size of the floating platform for a 100 MW-net output. The thermodynamic cycle is assumed to be a closed-cycle plant. The main properties of the plantship are summarized in Table 1.

The ship type was selected as a Suezmax crude oil carrier. Here, the hull geometry is assumed to follow the KVLCC2M form scaled to a Suezmax size. The inertia properties are roughly estimated by considering the plant layout. Note that the plant layout is highly dependent on the arrangement of the intake and discharge water pipes; it is assumed to be constant in this study. The hydrodynamic properties are computed by an in-house solver for hydrostatic, diffraction and radiation analyses based on the High-Order Boundary Element Method (HOBEM). This tool

Table 2. Main properties of the floating structures.

Properties	Value
Geometry	KVLCC2M
Length, L_{pp}	275 m
Breadth	50 m
Depth	29 m
Draught	17.9 m
Displacement	204,035 ton
Center of gravity above bottom, KG	13.9 m
Radius of gyration, k_{xx}	14.0 m
Radius of gyration, k_{yy}	62.9 m
Radius of gyration, k_{zz}	64.6 m

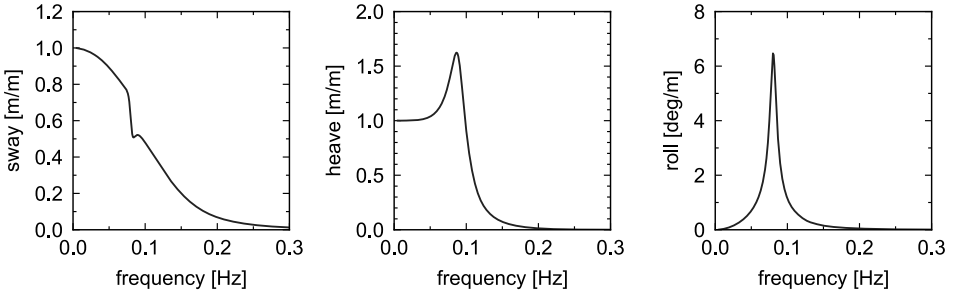

Fig. 2. Response amplitude operator of the floating structure without mooring and the CWP.

also calculates mean wave drift forces and the Quadratic Transfer Function (QTF) are evaluated with Newman's approximation. Furthermore, wind forces, current forces, and viscous roll damping forces are evaluated using empirical formulae. Further details are reported by Hisamatsu.[34] The main dimensions and the Response Amplitude Operator (RAO) in beam seas condition are shown in Table 2 and Fig. 2, respectively.

A spread mooring system with 12 taut legs was designed for this concept. The arrangement of the mooring lines is shown in Fig. 3. Each mooring line consists of polyester rope, as presented in Table 3.

The deep seawater intake system consists of a single CWP with an inner diameter of 12 m and a design flow velocity of 2.1 m/s. The structural design of the CWP is summarized in Table 4. The CWP is assumed to be a solid-wall pipe fabricated of GFRP and its cross-sectional stiffness properties referred from the literature[5] are shown in Table 4. Note that the detailed structural design, including the connections, stiffeners, and fiber arrangements, is not discussed here.

The water-discharge system comprises four discharge pipes with an inner diameter of 10 m. This concept is based on discharging the seawater used for heat exchange

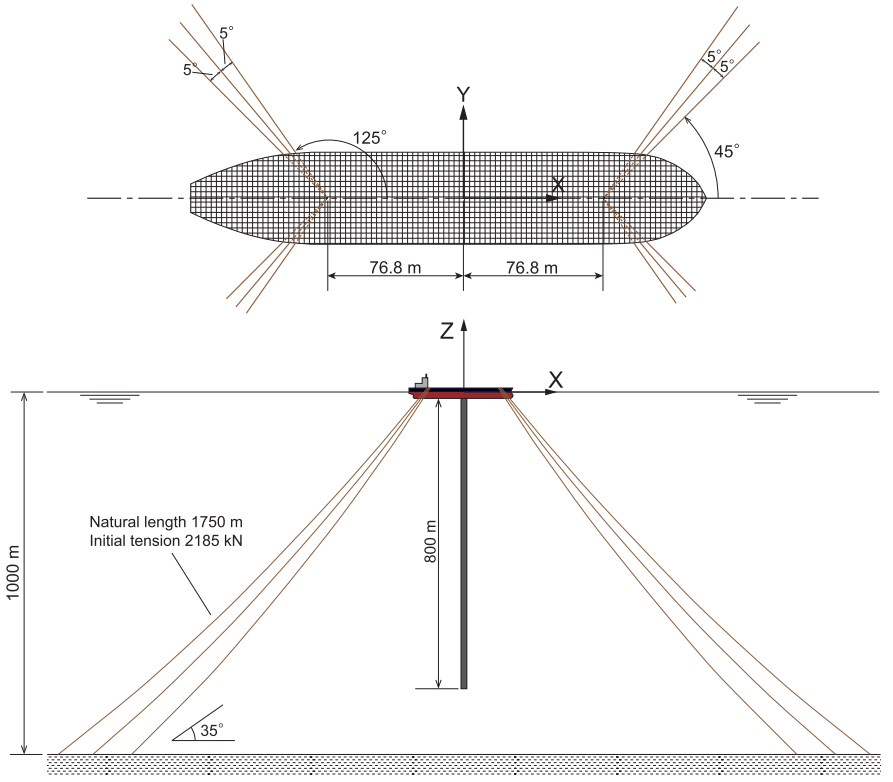

Fig. 3. Mooring layout of the baseline design.

Table 3. Main properties of mooring line.

Properties	Value
Line type	Polyester rope
Nominal diameter	212 mm
Axial stiffness	294 MN
Minimum Breaking Load (MBL)	12,263 kN
Weight in seawater	7.52 kg/m
Normal added mass coefficient	1.0
Normal drag coefficient	1.6

into a layer having the same temperature as the discharge water; therefore, the pipe length is set to 100 m. The dynamic interaction hanging pipes of this length and the floating platform can be neglected as long as the pipe is connected to the platform with pinned joints. Thus, the discharge pipes are not considered in this paper.

Table 4. Main properties of baseline Cold Water Pipe (CWP).

Properties	Value
Length, L	800 m
Inner diameter, D_i	12.00 m
Outer diameter, D_o	12.32 m
Design flow velocity, u	2.1 m/s
Material	GFRP
Material density, ρ	1.52 t/m^3
Tensile modulus, E	13,776 MPa
Yield stress, σ_Y	550 MPa

3. Design Modification of the CWP

This section evaluates the impact of changing the CWP design on the power output and cost of the floating OTEC plant. In this paper, the following structural categories remain unchanged from the baseline design: solid-wall pipes fabricated solely of GFRP, hanging condition, with the top pinned, and the bottom free, connected at the bottom of the floating platform, and pipe not bundled. Accordingly, the CWP design is parameterized in terms of

- the length, L,
- the inner diameter, D_i,
- the outer diameter, D_o, or the wall thickness, t,
- the internal flow velocity, u,
- the number of CWPs, N.

3.1. *Evaluation method of hydraulic performance and cost*

According to the plant model formulated by Uehara and Ikegami,[35] the power output from an OTEC plant is expressed as

$$P_n = P_g - W_f - W_w - W_c, \tag{3.1}$$

where P_n, P_g are the net and gross power outputs, respectively, and W is the pumping power. Here, subscripts 'f', 'w', and 'c' denote the working-fluid, warm-water, and cold-water circuits, respectively. This formula indicates that a portion of the electricity generated by the turbine is consumed by the pumps. Thus, the effective output from the overall plant is reduced from the turbine output.

The direct impact on the cost of changing the CWP design would be considered as: the material cost related to the material volume of the structure, the fabrication and installation costs, a change in the pumping power W_c, a change in the cold water temperature due to heat transfer through the CWP wall. An indirect effect is considered to be a change in the plant arrangement due to a change in the layout of the CWP and the resulting changes in the pumping power. In the direct effect, the

modeling fabrication and installation costs is difficult due to the lack of experience. Furthermore, the effect of heat loss is negligible unless the diameter is small and the flow velocity is very low.[36] Therefore, this study concentrates on the effects of material cost and pumping power.

As discussed above, the plant configuration and power output from the turbine are assumed to be fixed. To keep the cold seawater temperature, the CWP length L is thus fixed. Hence, the design parameters of the CWP to be considered in this evaluation are the inner diameter D_i, the wall thickness t, flow velocity u, and number of pipes N. Considering this design constraint, the pumping power regarding the CWPs is expressed as the entrance pressure loss and the frictional loss:

$$W_{\text{cwp}} = \left(k + f\frac{L}{D_i}\right)\frac{\rho S_i u^3}{2\gamma}, \tag{3.2}$$

where k and f are the entrance and frictional loss coefficients, respectively, ρ is the seawater density, S_i is the hydraulic area ($S_i = \pi/4D_i^2$), and γ is the pump efficiency. For a straight inlet, the entrance kiss coefficient is approximately $k = 1.0$. The frictional loss coefficient is evaluated using the Colebrook formula. Although the pump efficiency depends on a flow rate and water head, a constant efficiency of $\gamma = 0.9$ is assumed in this study. Using this assumption, the net output P_n is estimated based on how much the head loss deviates from the baseline design.

To evaluate the capital cost of the CWP, the wall thickness is first fixed at a constant ratio to the inner diameter, $D_i/t = 60$, for all design cases. The capital cost of the CWP for a 100-MW-scale plant is estimated from the literature[37] to be 5% of the total capital cost of the plant. Here, the cost variation is considered to be proportional to the total volume of GFRP.

The effect of changing these design variables on the cost is evaluated using the Levelized Cost Of Energy (LCOE) model:[37]

$$\text{LCOE} = \frac{C + \sum_{i=1}^{n}[M_i/(1+r)^i]}{\sum_{i=1}^{n}[P_i/(1+r)^i]}, \tag{3.3}$$

where i is the year from the start of the project, r is the discount rate, n is the project life, C is the Capital Expenditure (CAPEX), M_i is the Operation and Maintenance Expenditure (OPEX) at year i, and P_i is the annual electricity production, that is assumed by $P_i = cP_n$, where c is the annual capacity factor and the rated power output P_n. Here, we assume a discount rate of 10%, a plant life of 20 years, a capacity factor of 95%, and the OPEX is 5% of the CAPEX. Furthermore, the capital expenditure of CWP with the baseline design is assumed to be 5% of the total CAPEX. The LCOE of the baseline design is considered as \$0.2/kWh withs a 30% uncertainty band.[37]

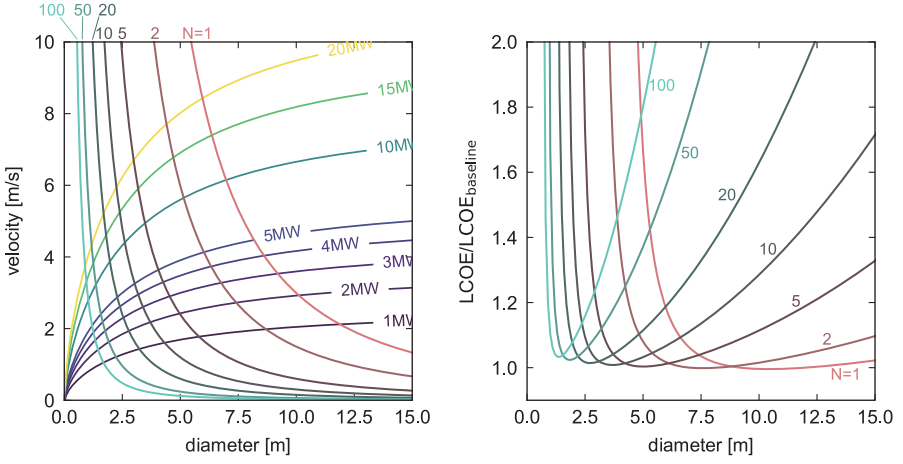

(a) (b)

Fig. 4. Design space of multiple CWPs: N is the number of CWPs; Q is the flow rate; $\mathrm{LCOE}_{\mathrm{baseline}}$ is the cost of baseline design, \$0.2/kWh.

3.2. *Design space exploration*

To discuss the design trade-offs, this section presents the design space with the inner diameter D_i, the internal flow velocity u and the number of CWPs N. Figure 4 illustrates the set of possible designs and the estimated cost. Figure 4(a) shows the power loss as a function of D_i and u. In general, increasing the internal flow velocity allows for a smaller inner diameter, although it leads to a significant increase in head loss. As a result, the cost increases rapidly as shown in Fig. 4(b). Conversely, increasing the inner diameter by reducing the internal flow velocity raises the cost because of the substantial increase in material volume. Consequently, there exists a theoretical optimal combination of D_i and u for each number of CWPs.

Importantly, while the optimal cost increases with increasing the number of CWPs, the increase is very slight. Figure 5 summarizes the optimal configurations

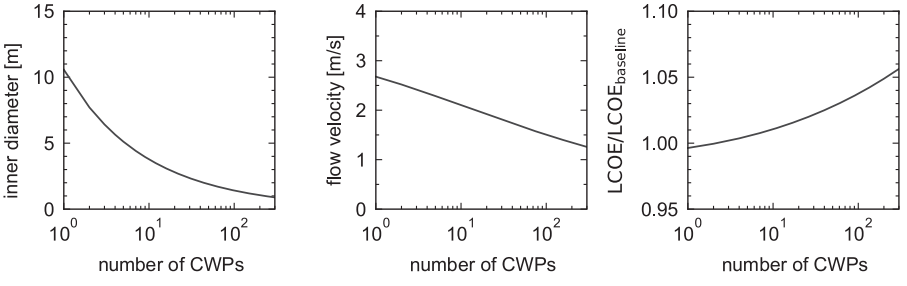

Fig. 5. Optimal configurations of the CWPs (fixed at $D_i/t = 60$).

of the CWP design. For example, in the case of $N = 100$ with a diameter of 1.34 m, only 3% higher than the baseline design. Considering the uncertainty in cost and pump efficiency, these values could be considered negligible. This conclusion has also been mentioned by Langer *et al.*[31]

Moreover, the design sensitivity to the number of CWPs becomes higher as the inner diameter decreases. This indicates that the number of CWPs increases sharply when the inner diameter is less than approximately 3 m. Although this factor was not included in the optimization, considering the increase in lead time and construction cost, the result may be disadvantageous when designing multiple smaller-diameter CWPs.

3.3. *Evaluation of structural dynamic response*

In this section, the dynamic structural response characteristics of the floating OTEC plant are analyzed based on the optimal design configurations identified in the previous section. The analysis is conducted using a simplified model previously developed by the authors.[23] The model has been extended to account for multiple CWPs. It linearizes the coupled system consisting of the floating body, mooring system, and CWPs, and approximates the system in two dimensions. Therefore, the dynamic response is evaluated in the frequency-domain. This modeling approach has been found to yield results that are generally consistent with those obtained from time-domain nonlinear dynamic analysis.

The extreme environmental condition considered in this study is the beam sea, in which waves, winds, and currents approach the platform from 90°. The environmental conditions are assumed to represent a low-latitude site without typhoons. Furthermore, considering the characteristics of the spread mooring system, in which the bow faces the predominant wave and wind direction, the significant wave height of the transverse waves is assumed to be smaller.

The waves are modeled as a JONSWAP spectrum with a significant wave height of $H_s = 3.65$ m, a peak period of $T_p = 11.1$ s and a peak factor of $\gamma = 2.79$. The winds are modeled a uniform profile with a wind speed of 28.6 m/s. The currents are represented as a steady flow and the profile assumes the 1/7 law using a surface speed of 0.85 m/s. These environmental conditions are used in the static analysis, the equivalent linearization of drag forces, and the estimation of slowly-varying wave drift motion.

The structure of the CWP is assumed as a GFRP solid-wall pipe. In this analysis, the wall thickness is varied such that the ratio of D_i/t is set to 50, 60, 70, 80, and 100. All CWPs are assumed to be located at the bottom center of the platform. The hydrodynamic characteristics of the CWP in the currents and waves depend on the Reynolds number, the roughness, and the Keulegan–Carpenter number, $\mathrm{KC} = U_m T/D$, where, U_m is the velocity amplitude of an oscillation flow, T is the period, and D is the diameter of a circular cylinder. The drag coefficient C_d and added mass

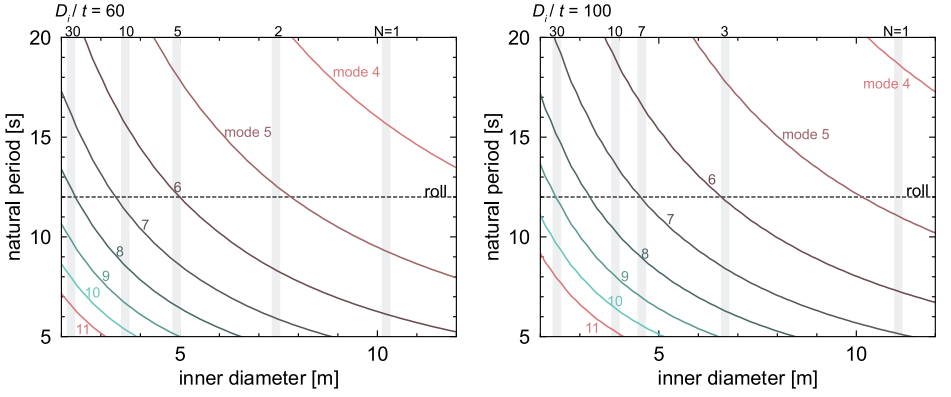

(a) (b)

Fig. 6. Natural period of lateral vibration of the CWP varying with the inner diameter at $D_i/t = 60$ and 100.

coefficient C_a are calculated using the empirical formula following DNV-RP-C205.[38] In this case, C_d increases and C_a decreases as the diameter decreases.

The dominant response of the CWP is bending vibration induced by platform motion in waves. Hence, the coupling between the natural frequencies of each component and the wave frequencies is one of the main concerns in the structural design. Figure 6 shows the variation of natural frequencies with the number of CWPs. The critical frequency range is around the natural frequency of roll ($T = 12$ s), which is indicated by the dashed line in Fig. 6. Accordingly, the 5th–7th modes in configurations with $N = 2$–10 (corresponding to the inner diameters of 4–7 m) would be excited by the platform motion. In contrast, since the lower-order modes (below the 3rd mode) of the CWP have natural periods longer than 25 s for all configurations, a serious resonance is unlikely to occur in the design cases examined in this section.

The frequency response of the platform–CWP coupled system under wave excitation is shown in Fig. 7. Here, the CWP's frequency response is represented by a value evaluated by

$$\sigma_{\mathrm{rms}}(f) = \sqrt{\frac{\int_0^L |\sigma_A(f;x) + \sigma_B(f;x)|^2 dx}{L}}, \tag{3.4}$$

where σ_{rms} is the representative bending stress along the CWP, σ_A and σ_B are the mean axial stress and bending stress at the outer surface, respectively, as function of the wave frequency f and the local coordinate x.

The sway and roll motions of the platform are affected by the dynamic coupling with the bending modes of the CWPs in all design cases. In contrast, the heave response remains unchanged because the total mass of the CWPs does not vary significantly among the cases. Pronounced peaks appear in the low-frequency range

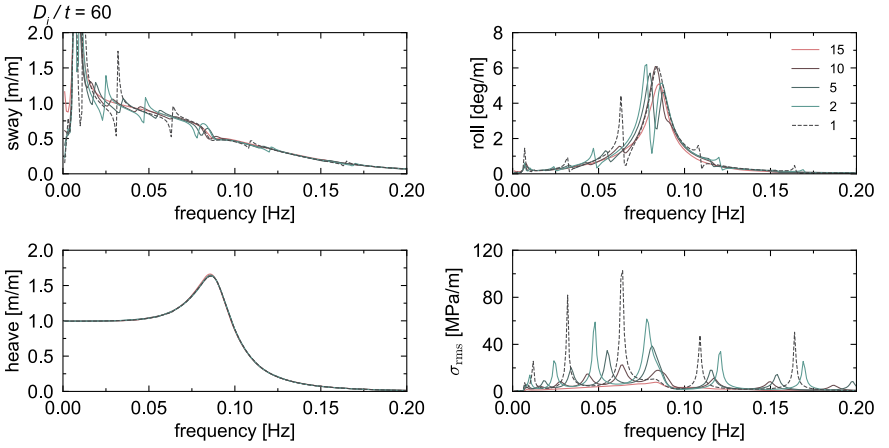

(a)

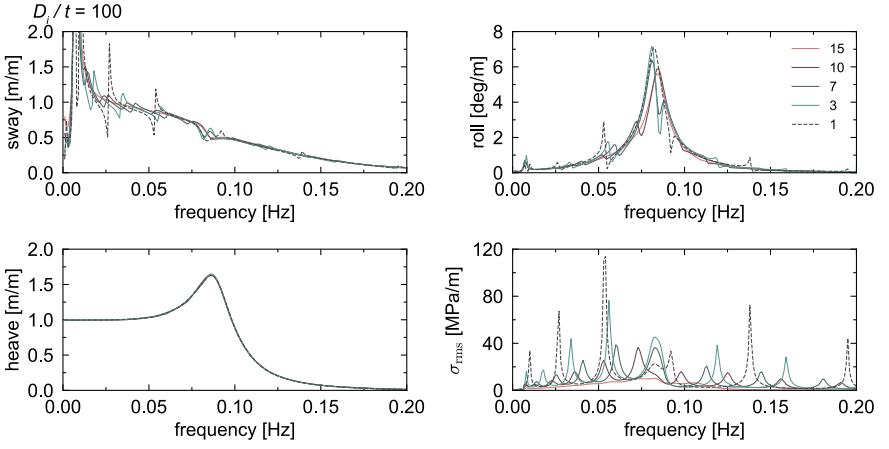

(b)

Fig. 7. Coupled RAO at $D_i/t = 60$ and 100; each line are the number of CWPs, N.

of the sway and roll responses in Fig. 7. These peaks are induced by the dynamic coupling with the CWP modes, and they become more pronounced as the CWP diameter increases. This is because larger-diameter pipes couple with lower-order bending modes, which possess greater modal mass. In this case, the stress amplitude of the CWP also increases. In contrast, for smaller-diameter pipes, where higher-order bending modes are excited and drag-damping is large, the resulting stress is not significant.

In particular, the roll resonance can be strongly affected when the decoupled natural periods of the roll and CWP bending modes are close. As shown in Fig. 8,

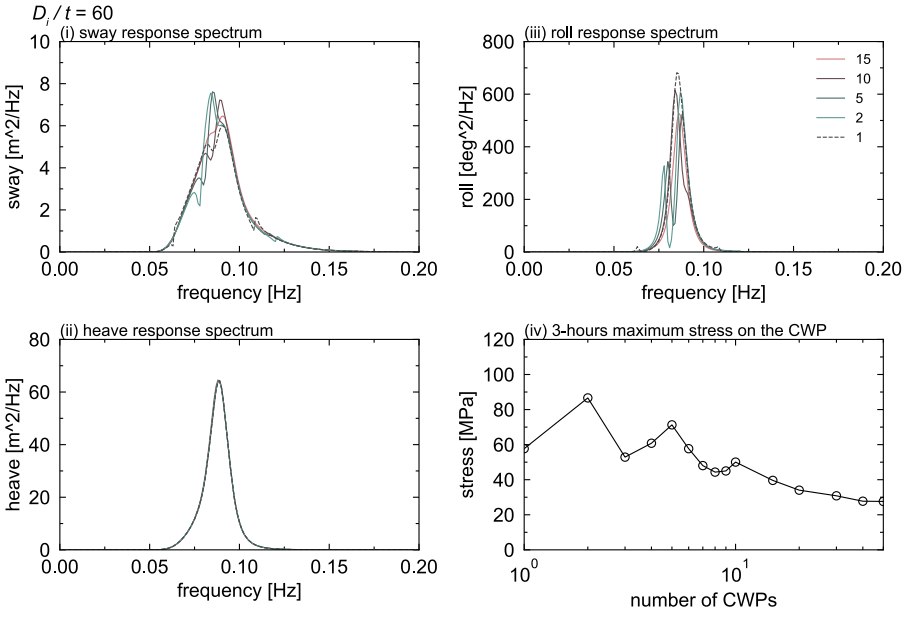

(a)

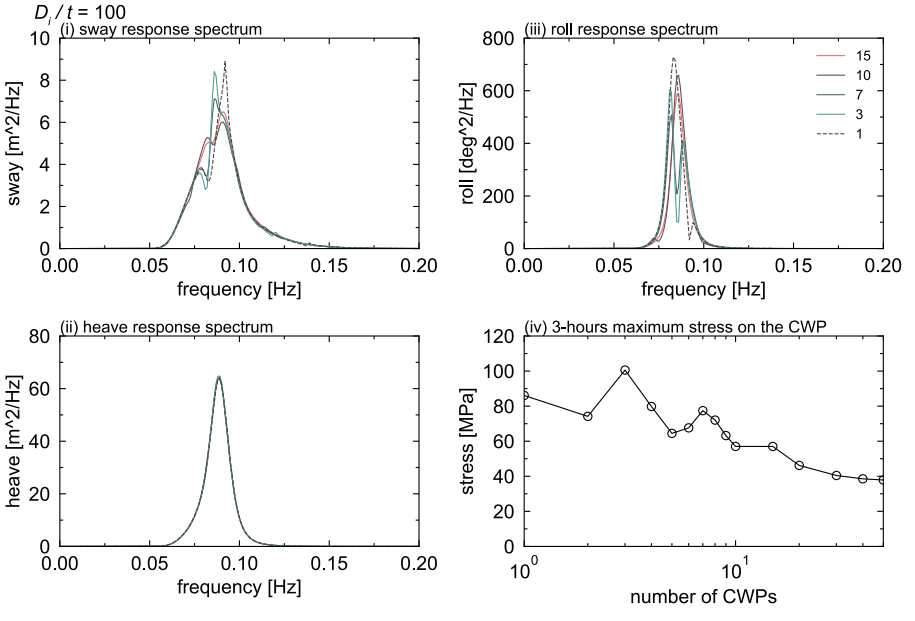

(b)

Fig. 8. Response spectrum and 3-h maximum stress on the CWP varying with the number of CWPs; each line are the number of CWPs, N.

a notable coupling response around the roll natural period appears for $N = 2$ at $Di/t = 60$ and for $N = 3$ at $D_i/t = 100$, where the respective 5th and 6th bending modes are close to the roll natural period. In such cases, strong inertial coupling splits the original roll peak into a double-peak response, and the CWP response also increases significant

The resulting response spectra and the 3-h probable maximum values estimated using the Rayleigh distribution are shown in Fig. 8. For $D_i/t = 60$, the largest stress on the CWP occurred at $N = 2$ and $N = 5$, corresponding to strong interactions between the roll and the 5th and 6th CWP modes, respectively. For $D_i/t = 100$, the largest response occurs at $N = 3$ and $N = 7$, corresponding to interactions between the roll and the 6th and 7th CWP modes. In both cases, the peak CWP response appears when the decoupled natural periods of the roll approach those of the CWP bending modes.

The current force and hydrodynamic drag acting on the CWPs have a significant impact on the mooring design, as shown in Fig. 9. As the number of CWPs increases, both the total projected area and the drag coefficient increase, leading to a higher steady environmental load on the mooring system. Consequently, increasing the number increases the static mooring tension. However, Fig. 9 also shows a significant increase in dynamic mooring tension for $N = 1$, which results from the strong coupling between the lower-order CWP modes and the slowly varying wave-drift motion of the moored platform. For $D_i/t = 60$, the decoupled second bending mode of the CWP has a natural period of $T = 144\,\mathrm{s}$, which is close to the sway natural period of $T = 143\,\mathrm{s}$, whereas for $D_i/t = 100$, the corresponding period is $T = 184\,\mathrm{s}$. In the former case, the large modal mass of the second bending mode

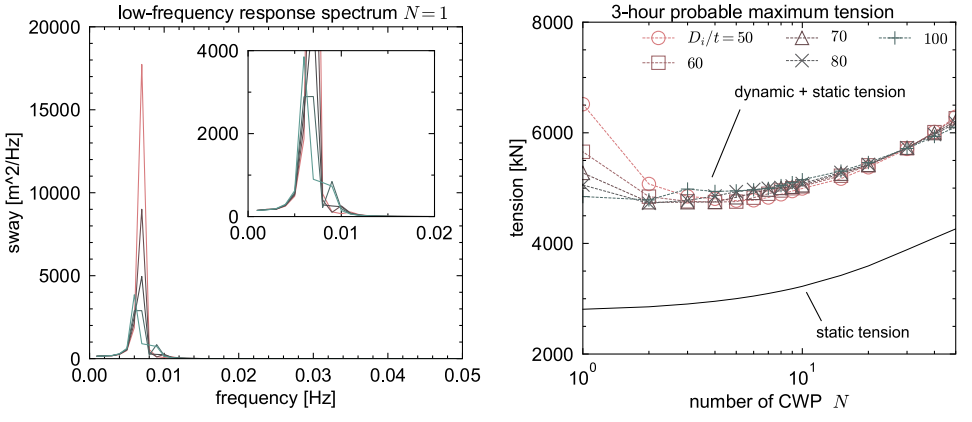

(a) (b)

Fig. 9. Low-frequency sway response and 3-h maximum mooring tension varying with the number of CWPs.

of the CWP significantly amplifies the coupled frequency response function. As the number of CWPs increases, drag-damping effects become dominant, reducing the influence of the inertial coupling on the response characteristics.

4. Structural Feasibility Analysis

In the previous section, the structural characteristics of multiple CWPs were comprehensively examined. In this section, their feasibilities are evaluated using the time-domain simulation with OrcaFlex 11.4c. This analysis enables more rigorous evaluation of hydrodynamic loads and the dynamic tension in the mooring lines, as well as the nonlinearity of the hydrodynamic loads acting on the CWPs.[23]

The representative design configurations of the CWPs are as follows:

- $L = 800\,\text{m}$, $D_i = 12.0\,\text{m}$, $D_o = 12.32\,\text{m}$ ($D_i/t = 75$), $N = 1$ (baseline);
- $L = 800\,\text{m}$, $D_i = 5.0\,\text{m}$, $D_o = 5.17\,\text{m}$ ($D_i/t = 60$), $N = 5$;
- $L = 800\,\text{m}$, $D_i = 3.0\,\text{m}$, $D_o = 3.10\,\text{m}$ ($D_i/t = 60$), $N = 15$;
- $L = 800\,\text{m}$, $D_i = 2.0\,\text{m}$, $D_o = 2.067\,\text{m}$ ($D_i/t = 60$), $N = 39$.

The first and second examples represent scenarios that require investment in dedicated manufacturing equipment. The next example, with a diameter of 3 m, is regarded as the currently feasible diameter.[32] The 2 m diameter may correspond to a scenario in which commercially available products can be readily procured. Smaller diameters may also be possible; however, considering the requirements for discharge pipes and hull reinforcement, the minimum practical CWP diameter for a 100 MW-scale plant is considered to be approximately 2 m in this study.

The arrangement of the CWPs is a significant factor affecting the risk of contact. Therefore, a preliminary study is first conducted using the CWP arrangement shown in Fig. 10. For the designs with $N = 1,\ 5,\ 15$, the CWPs are arranged along the hull centerline with a minimum separation of $3D_i$ between adjacent pipes. For the case of $N = 39$, arranging all pipes along the centerline is impractical; therefore, the CWPs are positioned in two parallel rows symmetrically on both sides of the centerline.

This section considers the Ultimate Limit State (ULS). The maximum structural response is evaluated under extreme environmental conditions corresponding to a 50-year return period. The environmental conditions are identical to those used in the previous section. The extreme values are obtained using 10 random seeds, with each time-domain simulation running for 3 h (10,800 s).

Figure 11 shows the results of the maximum sway of the hull and the tension of the mooring. The mooring tensions for all design cases remain below 60% of the Maximum Breaking Load (MBL), satisfying the intact mooring design criteria specified in ISO 19901-7.[39]

The significant increase in sway and mooring tension, as shown in Fig. 11, is attributed to increasing current forces acting on the pipe array. This conclusion is

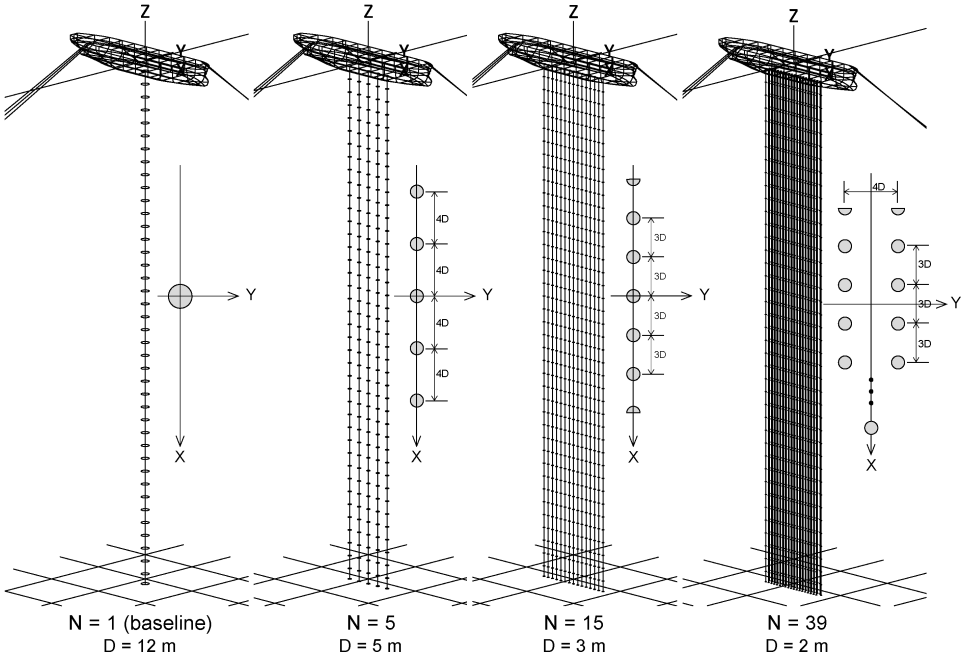

Fig. 10. Design examples of CWP arrangement: N is the number of CWPs; D is the inner diameter.

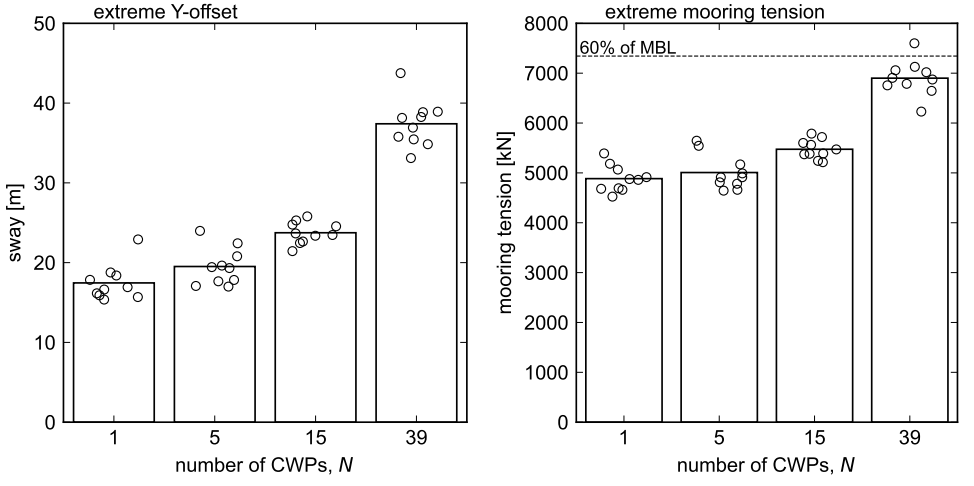

(a) (b)

Fig. 11. Extreme value of sway and mooring tension: the bar is the mean value of 10 times simulations; the scatter plot is each maximum values.

consistent with that obtained with the simplified model discussed in previous section. However, the significant increase observed in the single-CWP case in Fig. 9 is not seen in Fig. 11, which is obtained using a higher-fidelity approach. A possible explanation is that the case of $D_i/t = 75,\ N = 1$ does not significantly amplify the slowly-varying sway response, because the coupling between the sway and CWP modes is relatively weak. Additionally, the hydrodynamic forces acting on the mooring lines, which are not considered in the simplified model, would change the natural period, the damping effect and the resulting response of the coupled system. Another important aspect is the displacement of the CWPs induced by current forces. For the lightest and most flexible 2-m CWPs, it is observed a lower-end displacement of 266 m. These results highlight the necessity of considering such displacements when designing CWPs for sites with strong currents.

The maximum von Mises stress and the minimum CWP's clearance are shown in Fig. 12. Figure 12(b) indicates that the relative motion between adjacent pipes is practically negligible. Since the higher-order elastic modes mainly govern the CWP's response, the risk of contact between CWPs is minimal. In principle, clearance could occur if the first bending mode were excited, as it involves large lateral motion and phase difference. However, the first natural period exceeds 300 s for all deign cases, and no such behavior is observed.

As discussed in the previous section, the modal properties of CWPs change significantly as their diameter decreases. Smaller-diameter CWPs can avoid resonance in the lower-order modes, thereby reducing the stress response. Consequently, the

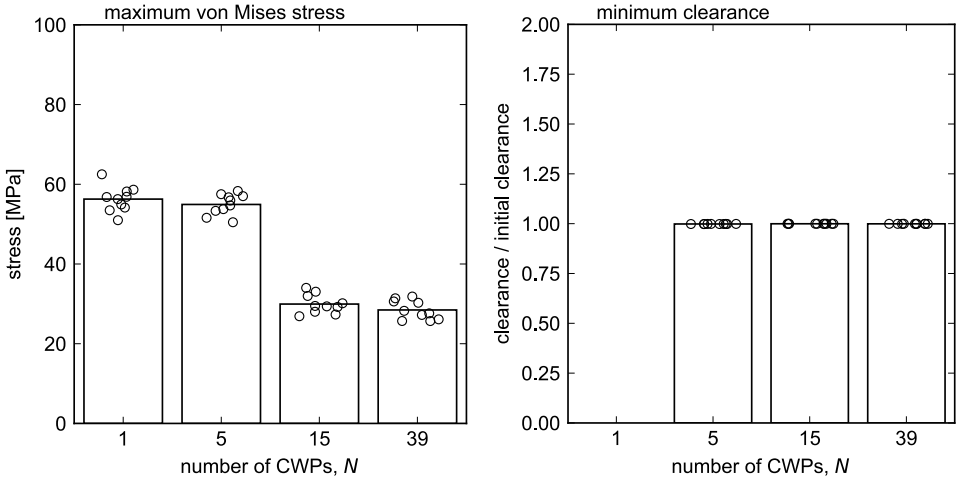

(a) (b)

Fig. 12. Extreme value of von Mises stress and pipe's clearance along the CWP: the bar is the mean value of 10 times simulations; the scatter plot is each maximum values.

case of $N = 15$ and $N = 39$ exhibit lower stress levels than the larger-diameter CWP configurations, as shown in Fig. 12(a). For larger-diameter CWPs, the stress remains below the yield stress of 550 MPa. In particular, for the case of $N = 5$, resonance occurs in the coupled mode of the roll and the 6th bending mode of the CWPs. Although the stress increases to a level comparable to that of $N = 1$ case, as seen in Fig. 12(a), the stress is still not critical for the ULS. As a result, the all design cases of the CWPs are considered feasible in the considered ULS.

5. Concluding Remarks

This paper has discussed the design trade-offs, dynamic characteristics and feasibility of a concept of multiple CWPs for an OTEC plantship. As a case study, a preliminary baseline design featuring a ship-shaped platform and a spread mooring system is considered. The CWP is assumed to be a solid-wall GFRP pipe.

The main conclusions of this study are as follows:

- Considering only the material cost and hydraulic head loss of the CWPs, the influence of the optimal configuration on overall economics is negligible.
- By modifying the diameter and wall thickness of the CWP, the natural frequency of bending vibration can be significantly shifted. For ship-shaped floating bodies, avoiding natural frequency conflict between the CWP bending modes and that of the rigid motion of the moored platform is effective in reducing bending stress of the CWP.
- For CWP configurations with diameters below 3 m, the bending stress induced by platform motion remains relatively small. However, current loads can have a considerable impact on both mooring design and CWP displacement.
- From a structural perspective, medium-diameter CWPs made of GFRP are considered to be feasible for deployment in low-latitude seas without tropical typhoons.

This study discusses the structural performance, focusing on a ship-shaped platform, which generally exhibits large motions. Although dynamic stresses would be reduced by adopting a semi-submersible or spar-type platform, it is necessary to examine whether multiple CWPs can be arranged on such platforms. In addition, GFRP was used for the CWPs in this study, whereas a High-Density Polyethylene (HDPE) CWP with a diameter of 3 m is currently regarded as a commercially available option.[32] In future work, it will be increasingly important to investigate lighter and more flexible HDPE CWPs.

This preliminary study suggested that a concept of the multiple CWPst is economically and technically feasible for a floating OTEC plant. However, in practical implementation, the cost of manufacturing and procuring CWPs for specific sites may become a dominant factor. Furthermore, as the diameter of the CWPs

decreases, fatigue due to current-induced-VIV, turbulent wake effects, and internal flow induced vibration is expected to become more significant in this field.

ORCID

Ryoya Hisamatsu https://orcid.org/0000-0002-8491-789X
Tomoaki Utsunomiya https://orcid.org/0000-0003-2081-7547

References

1. L. Vega, Ocean thermal energy conversion, in *Encyclopedia of Sustainability Science and Technology* (Springer, New York, NY, 2017), pp. 1–35.
2. B. Martin, S. Okamura, T. Yasunaga, Y. Ikegami and N. Ota, OTEC and advanced deep ocean water use for Kumejima: An introduction, in *OCEANS 2022* (IEEE, Chennai, India, 2022), pp. 1–5.
3. W. Gao, F. Wang, Y. Zhang, Z. Tian, D. Wu and S. Farrukh, Review of performance improvement strategies and technical challenges for ocean thermal energy conversion, *Appl. Therm. Eng.* **266** (2025) 125506, doi:10.1016/j.applthermaleng.2025.125506.
4. IEA-OES, White paper on ocean thermal energy conversion (OTEC), IEA Technology Programme for Ocean Energy Systems (OES), Lisbon, Portugal (2021).
5. G. C. Nihous and L. A. Vega, Design of a 100 MW OTEC-hydrogen plantship, *Mar. Struct.* **6**(2–3) (1993) 207–221, doi:10.1016/0951-8339(93)90020-4.
6. L. A. Vega and D. Michaelis, First generation 50 MW OTEC plantship for the production of electricity and desalinated water, in *Proc. Annual Offshore Technology Conf.*, Vol. 4, Texas, USA (2010), pp. 2979–2995.
7. B. Cable, OTEC system design report, Technical Report, Naval Facilities Engineering Service Center, CA, USA (2010).
8. B. Cable, OTEC technology development report, Technical Report, Naval Facilities Engineering Service Center, CA, USA (2010).
9. R. Adiputra, T. Utsunomiya, J. Koto, T. Yasunaga and Y. Ikegami, Preliminary design of a 100 MW-net ocean thermal energy conversion (OTEC) power plant study case: Mentawai Island, Indonesia, *J. Mar. Sci. Technol.* **25**(1) (2020) 48–68, doi:10.1007/s35128-020-0757-1.
10. J. Langer, J. Quist and K. Blok, Recent progress in the economics of ocean thermal energy conversion: Critical review and research agenda, *Renew. Sustain. Energy Rev.* **130** (2020) 109960, doi:10.1016/j.rser.2020.109960.
11. G. Nihous, A preliminary investigation of the effect of ocean thermal energy conversion (OTEC) effluent discharge options on global OTEC resources, *J. Mar. Sci. Eng.* **6** (2018) 25, doi:10.3390/jmse6010025.
12. W. H. Avery and C. Wu, *Renewable Energy from the Ocean: A Guide to OTEC* (Oxford University Press, Oxford, UK, 1994).
13. T. McGuinness, A. Griffin and D. Hove, Preliminary designs of cold-water pipes for barge- and spar-type OTEC plants, in *Proc. 6th Ocean Thermal Energy Conversion Conf.*, Vol. 1, Washington, D.C., USA (1979), pp. 6.1.1–6.1.12.
14. L. A. Vega and G. C. Nihous, At-sea test of the structural response of a large-diameter pipe attached to a surface vessel, in *Proc. Annual Offshore Technology Conf.*, Houston, Texas, USA (1988), pp. 473–480.

15. A. Miller and M. Ascari, OTEC advanced composite cold water pipe: Final technical report, Technical Report, Lockheed Martin MS2, USA (2011).
16. H. J. Kim, H. S. Lee, J. B. Seo, S. T. Lim, J. H. Moon and Y. S. Kim, Demonstration of 1MW OTEC plant in Korean waters in 2019, in *Proc. 7th OTEC Symp.*, Busan, Korea (2019).
17. K. Ouchi, K. Otsuka and H. Omura, Recent advances of ocean nutrient enhancer "TAKUMI" project, in *Proc. ISOPE Ocean Mining Symp.*, Hunan, China (2005), pp. 7–12.
18. J. R. Paulling, Frequency-domain analysis of OTEC CW pipe and platform dynamics, in *Proc. Annual Offshore Technology Conf.*, Houston, Texas, USA (1979), pp. 1641–1652.
19. W. K. Jawish, III and R. Scotti, Study of three OTEC cold water pipe design analysis computer models, in *Proc. 8th Ocean Energy Conf.*, Vol. 1, Washington, D.C., USA (1981), pp. 25–30.
20. R. A. Barr and L. R. Sheldon, Model testing of OTEC plant platform and cold water, in *Proc. Annual Offshore Technology Conf.*, Houston, Texas, USA (1980), pp. 85–92.
21. Bureau Veritas, *Classification and Certification of Ocean Thermal Energy Converter (OTEC) — Tentative Rules*, Bureau Veritas, France (2018).
22. IEC, *Marine energy — Wave, tidal, and other water current converters — Part 20: Design and analysis of an Ocean Thermal Energy Conversion (OTEC) plant — General guidance* (IEC TS 62600-20), IEC Geneva, Switzerland (2019).
23. R. Hisamatsu and T. Utsunomiya, Coupled response characteristics of cold water pipe and moored ship for floating OTEC plant, *Appl. Ocean Res.* **123** (2022) 103151.
24. J. Halkyard, R. Sheikh, T. Marinho, S. Shi and M. Ascari, Current developments in the validation of numerical methods for predicting the responses of an ocean thermal energy conversion (OTEC) system cold water pipe, in *Proc. ASME 2014 33rd Int. Conf. Offshore Mechanics and Arctic Engineering*, Vol. 7, San Francisco, California, USA, ASME (2014), OMAE2014-24636.
25. S. C. Hirao, J. Umeda, K. Kokubun and T. Fujiwara, Tank test and numerical simulation of spar type floating OTEC, in *Proc. ASME 2021 40th Int. Conf. Offshore Mechanics and Arctic Engineering*, Virtual, Online, ASME (2021), OMAE2021-62107.
26. P. Cao, S. Xiang, J. He, S. Kibbee and S. Bian, Advancing cold water intake riser design through model test, in *Proc. Annual Offshore Technology Conf.*, Vol. 4, Houston, Texas, USA (2015), pp. 3019–3033.
27. Y. J. Kwon, H. J. Kim and D. H. Jung, A study for forced oscillation experiment for OTEC riser under current, in *Proc. The Twenty-fifth Int. Ocean and Polar Engineering Conf.*, Kona, Hawaii, USA (2015), pp. 212–219.
28. J. Wang, S. Xiang, S. Fu, P. Cao, J. Yang and J. He, Experimental investigation on the dynamic responses of a free-hanging water intake riser under vessel motion, *Mar. Struct.* **50** (2016) 1–19, doi:10.1016/j.marstruc.2016.06.003.
29. R. Hisamatsu and T. Utsunomiya, Free vibration and stability of a fully submerged pipe aspirating water: An experiment and new physical insights, *J. Fluids Struct.* **116** (2023) 103789, doi:10.1016/j.jfluidstructs.2022.103789.
30. Y. Ma, Y. You, J. Zhang, K. Chen and A. Feng, Experimental study on dynamic stability of vertical cantilevered pipe aspirating fluid immersed in various water depths, *Ocean Eng.* **272** (2023) 113378, doi:10.1016/j.oceaneng.2022.113378.
31. J. Langer, C. Infante Ferreira and J. Quist, Is bigger always better? Designing economically feasible ocean thermal energy conversion systems using spatiotemporal resource data, *Appl. Energy* **309** (2022), 118414, doi:10.1016/j.apenergy.2021.118414.

32. IEA-OES, Ocean thermal energy conversion (OTEC) economics: Updates and strategies, IEA Technology Programme for Ocean Energy Systems (OES), Lisbon, Portugal (2024).
33. S. Kibbee, Ocean thermal energy conversion at SBM, in *SNAME 18th Offshore Symp.*, Houston, Texas (Society of Naval Architects and Marine Engineers, 2013), pp. 3–18.
34. R. Hisamatsu, Design method and dynamic response of floating ocean thermal energy conversion (OTEC) plant, PhD thesis, Kyushu University, Fukuoka, Japan (2023).
35. H. Uehara and Y. Ikegami, Optimization of a closed-cycle OTEC system, *J. Sol. Energy Eng.* **112** (1990) 247–256, doi:10.1115/1.2929931.
36. L. Mao, C. Wei, S. Zeng and M. Cai, Heat transfer mechanism of cold-water pipe in ocean thermal energy conversion system, *Energy* **269** (2023) 126857, doi:10.1016/j.energy.2023.126857.
37. IEA-OES, International levelized cost of energy for ocean energy technologies, IEA Technology Programme for Ocean Energy Systems (OES), Lisbon, Portugal (2015).
38. DNV, Recommended Practice: Environmental conditions and environmental loads, DNV, Norway (2017).
39. ISO, Petroleum and natural gas industries — Specific requirements for offshore structures — Part 7: Stationkeeping systems for floating offshore structures and mobile offshore units, ISO, Geneva, Switzerland (2013).